Intercomparison of hydraulic pressure measurements to 28 MPa using a single-piston gauge in the controlled-clearance, reentrant, and simple configurations

K. Jain
Pressure and Vacuum Division, National Physical Laboratory, New Delhi 110012, India

C. Ehrlich and J. Houck
Thermophysics Division, National Institute of Standards and Technology, Gaithersburg, Maryland 20899

(Received 9 December 1991; accepted for publication 21 January 1992)

The use of controlled-clearance piston gauges as highly accurate primary pressure standards is well established. However, the operation of a controlled-clearance gauge is more complicated than that of the familiar simple or reentrant designs. An investigation has been performed on a modified design of a piston gauge for which the same piston/cylinder can be operated in either the controlled-clearance, simple, or reentrant modes, to determine the degree of degradation in accuracy of measured pressure using the gauge in either the simple or reentrant modes as a standard. How the particular characterization of the standard gauge affects the calibration parameters of a test gauge is also explored. The effective areas of the test gauge are within 4.5 parts per million (ppm) when the standard is used in the simple mode instead of the controlled-clearance mode, up to a pressure of 28 MPa, whereas in the case of the reentrant mode this deviation increases from 2.5 ppm at 7 MPa to 14 ppm at 26 MPa.

I. INTRODUCTION

The accurate measurement of pressure is required not only in industry, but also to study various physical and chemical phenomenon. Both piston gauges and liquid column manometers are used as primary pressure standards; the major difference is that the use of the latter is usually limited to near the atmospheric pressure region, whereas the former can be used over a wide range of pressures, from a few kPa to several hundred MPa.

In piston gauges, a cylindrical piston rotates in a well-fitted circular cylinder. The pressure at the base of the piston is determined as the ratio of the total downward force on the piston to the effective area of the piston/cylinder combination when the piston is floating at its operating level. The accuracy with which a pressure measurement can be made using these gauges depends on the accuracy with which measurements of both force and effective area can be made. The effective area of a piston gauge at low (atmospheric) pressure can be known to an estimated accuracy as high as several parts per million (ppm), and is essentially limited by the accuracy with which absolute dimensional measurements can be made on the piston and cylinder, although differences having to do with assumptions made in the model for the effective area can be significant.[1] The effective area at higher pressures changes with the applied pressure due to the elastic distortion of both the piston and the cylinder. Different ways of dealing with the pressure coefficient and hence the effective area have led to various piston gauge designs, various materials from which the piston and cylinder are made, and various pressure ranges for which they are to be used.[1] The elastic distortion of the cylinder is in general larger than that of the piston, at least for gauges of the "simple" design, in which the pressurizing fluid acts only on the interior (and sometimes end) surface of the cylinder. In gauges of the "reentrant" design, the pressurizing fluid acts over some or all of the outer surface of the cylinder as well, varying the overall distortion of the cylinder and complicating the ability to measure or predict it. At higher pressures, the estimated accuracy of the pressure measured by a gauge is mainly limited by how precisely the pressure distortion coefficient can be determined.

In a primary "controlled-clearance" piston gauge the elastic distortion of the cylinder is controlled by applying an independent pressure (jacket pressure p_j) to the outer surface of the cylinder.[2] The distortion of the piston can be calculated from theory using only the elastic properties of the piston material. The operation of the controlled-clearance piston gauge has the drawback, however, that it is more complicated and more time consuming than operation of the other types of piston gauges, leading to greater risk of errors because of the larger number of operating parameters. It is therefore desirable to be able to perform a primary characterization of a controlled-clearance gauge, but subsequently operate the gauge as a standard in a less complicated fashion while retaining the primary characterization parameters with minimal loss of accuracy. A gauge possessing such a capability might also be used to provide useful information concerning the observed phenomenon[3] where experimentally determined pressure distortion coefficients for the same test gauge are found to differ by as much as 20%–30%, which is outside the respective uncertainties, depending on the type of standard gauge used to perform the calibration. Attempts have been made in the past[4] to investigate similar effects using a standard gauge in the simple and reentrant modes.

In the investigation reported here, a piston gauge has been designed and developed in such a way that the system can be operated in the controlled-clearance, reentrant, or simple configurations while keeping the piston-cylinder

 0034-6748/92/053127-09$02.00

combination *in situ*, and without changing the position of the piston relative to the cylinder. A systematic and detailed study has been carried out with this gauge to study the behavior of the low-pressure effective area and the pressure distortion coefficient of a "simple" test piston gauge, designated as NIST3. This gauge was cross floated[2,5] against the standard gauge, which is designated as NIST1C when operated in the controlled-clearance mode, as NIST1R when operated in the reentrant mode, and as NIST1S when operated in the simple mode. The values of the low-pressure effective area and the pressure distortion coefficient thus obtained are also compared to the values obtained by the independent calibration of NIST3 against another pressure standard having a reentrant type of piston-cylinder assembly, designated NIST2. All of the parameters associated with the test gauge NIST3 will be referenced to the values obtained using the standard gauge in the controlled-clearance configuration (i.e., NIST1C).

II. THEORY

The pressure (P) generated at the reference level of a piston gauge is given by

$$P=\left[\sum_{i=1}^{n} M_i\left(1-\frac{\rho_{\text{air}}}{\rho_i}\right)g+\gamma C\right]\Big/[A_e(P)], \tag{1}$$

where M_i is the true mass of the ith weight, ρ_{air} is the density of air in the vicinity of the piston, ρ_i is the density of the ith weight, g is the local acceleration due to gravity, γ is the surface tension of the operating fluid, C is the circumference of the piston, and A_e is the effective area of the gauge.

The effective area ($A_{e(c)}$) of a controlled-clearance piston gauge is typically expressed as[2]

$$A_{e(c)}=\pi r_p^2(1+b_pP)[1+d(P_z-P_j)][1+(\alpha_p+\alpha_c)\times(T-T_r)], \tag{2}$$

where r_p is the piston radius at the reference temperature for low applied pressure, b_p is the pressure distortion coefficient of the piston, P is the pressure at the reference level of the piston, α_p is the linear thermal expansion coefficient of the piston, α_c is the linear thermal expansion coefficient of the cylinder, T is the absolute temperature of the piston and cylinder, T_r is the absolute reference temperature at which the gauge was characterized, d is the jacket pressure coefficient, P_z is the jacket pressure for which the clearance between the piston and cylinder is reduced to zero, and P_j is the operating jacket pressure. In the characterization of a controlled-clearance gauge, these parameters can either be measured or determined from knowledge of the mechanical properties of the materials from which the piston and cylinder are made. In practice, r_p, T, d, P_z, and P_j are usually measured, b_p is calculated, and α_p and α_c are usually obtained from the manufacturer.

If this same controlled-clearance gauge, which is now characterized, is to be used in the reentrant mode, where the jacket pressure is connected directly to the measured pressure, the equation for the effective area becomes

$$A_{e_{(r)}}=\pi r_p^2(1+b_pP)[1+d(P_z-P)][1+(\alpha_p+\alpha_c)\times(T-T_r)]. \tag{3}$$

If this same controlled-clearance gauge is used in the simple mode, there is no applied jacket pressure, and the expression for the effective area then becomes

$$A_{e_{(se)}}=\pi r_p^2(1+b_pP)[1+dP_z]\times[1+(\alpha_p+\alpha_c)(T-T_r)]. \tag{4}$$

Alternatively, it is also possible to derive an expression for the effective area of a simple piston gauge, using a measurement of the gap between the piston and cylinder, as[1]

$$A_{e_{(st)}}=\pi r_p^2(1+h/r_p)(1+b_{p/c}P)\times[1+(\alpha_p+\alpha_c)(T-T_r)], \tag{5}$$

where h is the gap width between the piston and cylinder for low applied pressure and $b_{p/c}$ is the pressure distortion coefficient of the piston and cylinder combination, which can be determined from knowledge of the mechanical properties of the materials from which the piston and cylinder are made.[2] In practice, it is nontrivial to measure h dimensionally, so that a hybrid scheme will be developed here which uses the controlled-clearance parameters to estimate h/r_p. This is done by noting that, experimentally, the expressions for d and P_z are usually not constants, but generally have a pressure dependence according to the expressions $d=D+\epsilon P$ and $P_z=P_{z0}+\sigma_z P$, where D, ϵ, P_{z0}, and σ_z are constants. Substituting these expressions into Eq. (4) and rearranging yields

$$A_{e_{(se)}}=\pi r_p^2(1+DP_{z0})(1+b_pP)[1+(D\sigma_z+\epsilon P_{z0})P]\times[1+(\alpha_p+\alpha_c)(T-T_r)], \tag{6}$$

where the addition and removal of terms second order in h/r_p are ignored. Comparison of Eqs. (5) and (6) shows that in both derivations the effective area for the gauge in the simple mode can be written as a product of the area of the undistorted piston, a constant term, a term containing a pressure dependence, and a temperature correction term. A hybrid equation containing the more easily (experimentally) obtainable components from each separate equation can then be written as

$$A_{e_{(sh)}}=\pi r_p^2(1+DP_{z0})[1+b_{p/c}P]\times[1+(\alpha_p+\alpha_c)(T-T_r)]. \tag{7}$$

From Eqs. (5) and (7) we can then see that the quantity h/r_p, which is difficult to determine from direct dimensional measurements, can also be obtained as the quantity DP_{z0} from controlled-clearance gauge measurements. Equations (2), (3), (4), and (7) are then used in this study to individually characterize the effective areas of piston gauge NIST1 in its different modes of operation, controlled-clearance (NIST1C), reentrant (NIST1R), simple experimental (NIST1S$_e$), and simple hybrid (NIST1S$_h$) respectively. The differences introduced into the calibra-

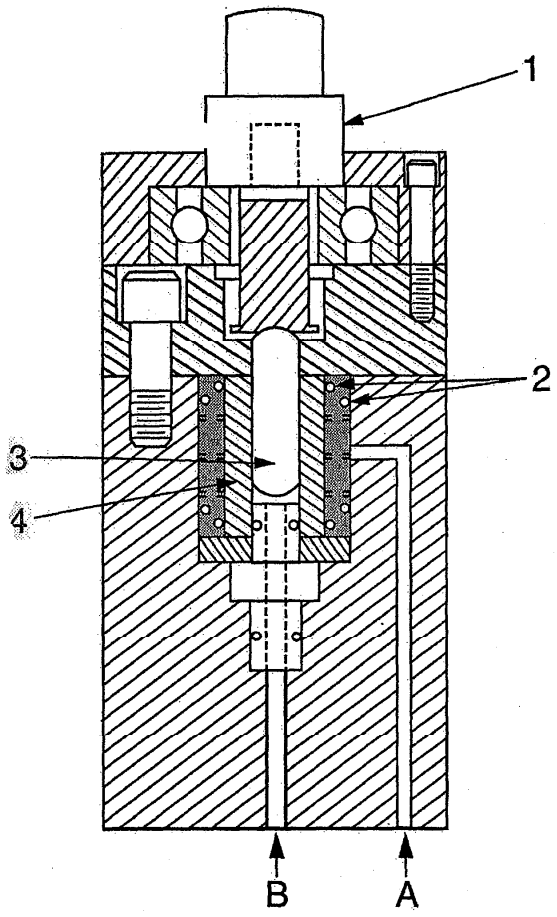

FIG. 1. Schematic cross-sectional view of the piston and cylinder mounting arrangement for the controlled-clearance primary pressure standard NIST1. (1) weight loading table, (2) O-ring, (3) piston, (4) cylinder, (A) jacket pressure, (B) measured pressure.

tion of the test gauge NIST3 using these individual characterizations of NIST1 as the standard gauge will be investigated.

III. EXPERIMENT

A schematic representation of the NIST-designed piston gauge NIST1, which has a modified commercially obtained piston and cylinder and is capable of generating full scale pressure to 28 MPa, is shown in Fig. 1. The novelty of the design is that the piston gauge can be used in either the controlled-clearance, reentrant, or simple modes to measure or generate pressure without the need to remove the piston or cylinder from the support column, or to disturb the position of the piston relative to the cylinder. The gauge is used in the controlled-clearance configuration by connecting the jacket pressure to port A and the measured pressure to port B. In the reentrant configuration port A and port B are connected together to the measured pressure, while in the simple configuration the measured pressure is again connected to port B, while port A remains open to the atmosphere.

Measuring the rate at which the piston sinks into the cylinder (fall rate) at different measured pressures allows a determination of the zero clearance jacket pressures. The radial clearance between the piston and the cylinder is directly proportional to the cube root of the piston fall rate. Fall rates were measured using a capacitance-type displacement transducer to avoid any extraneous force on the piston. The output of the transducer was directly recorded on an X-t chart recorder moving at a constant speed of 6 cm/min. A stopwatch was also used to time the fall rate independently. The change in position of the piston is known with a resolution better than 5×10^{-3} mm, and the time interval is determined to better than 0.2 s. The jacket pressure was measured using a Bourdon tube gauge (250 mm diameter) with an uncertainty of ±0.07 MPa.

Before starting the fall rate measurements, the entire system was leak checked by increasing the measured pressure (P_m) of NIST1C to 26 MPa. The piston was allowed to float for about an hour to allow the entire system to come to equilibrium and to establish thermal stability. At the time of the fall rate measurements the valve at the bottom of the piston was closed to isolate it from the rest of the pressure system. Twenty minutes were allowed for the system to attain equilibrium between two successive jacket pressure changes. At a particular jacket pressure (P_j), several observations of fall rate were taken. At any arbitrarily chosen load on the piston, P_j was increased until the time for the piston to fall through a fixed distance was long enough to be accurately measured. Fall times then were measured with increasing P_j using the same load on the piston until the curve of P_j as a function of the cube root of fall rate showed a deviation from linearity. The load was then increased and the fall rate measurements were made in a similar way for the new load.

The jacket pressure coefficient (d) of NIST1C was also determined experimentally by floating it against a tare piston gauge. At any load both piston gauges were brought to cross float equilibrium, i.e., their respective fall rates remain the same irrespective of whether the isolation valve between the gauges is closed or open, by adding additional fractional weight to the gauge which was generating the lower pressure. Then the jacket pressure was increased in steps, and the amount of extra load (ΔF) needed for each increase in jacket pressure (ΔP_j) to again bring both gauges back into the equilibrium condition was applied. The load (F) was then increased to the next higher value, and the same procedure was repeated. The jacket pressure coefficient was calculated at each load according to $d=(\Delta F/F)/\Delta P_j$. A first-order polynomial was fit to the data to show the dependence of d upon F.

For the calibration of the test gauge NIST3 using either NIST1 in any one of the piston-cylinder configurations or NIST2 as the standard, the well-established cross float method was used.[2,5] Each piston gauge was leveled to ensure the verticality of the axis, and the systems were checked for leaks to the full-scale pressure value of 28 MPa and were brought to cross float equilibrium, as discussed

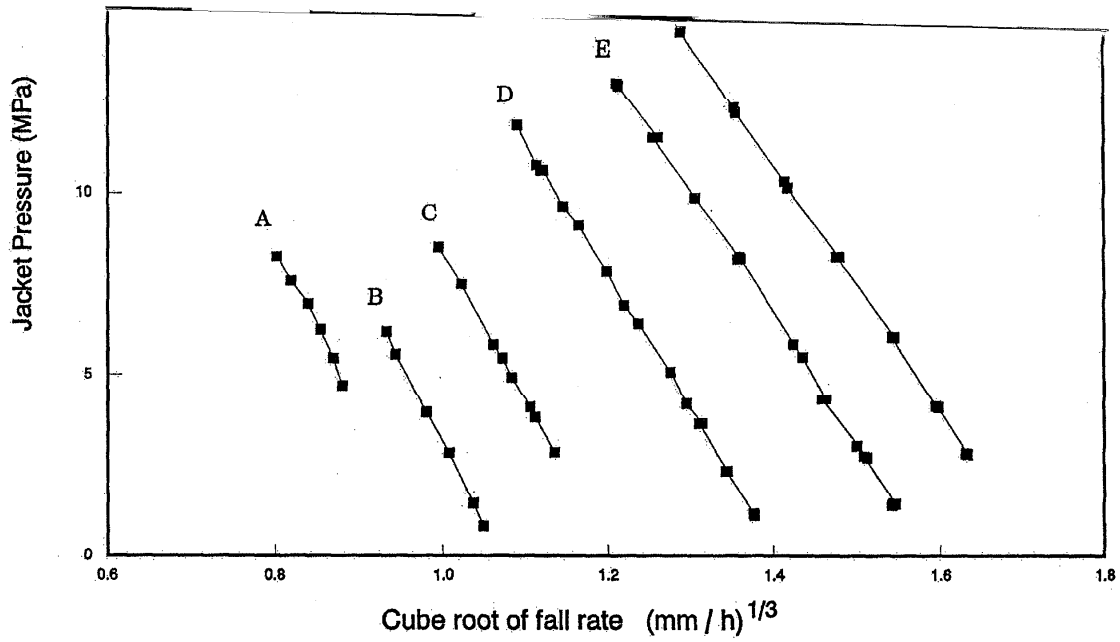

FIG. 2. Graph of jacket pressure (P_j) as a function of the cube root of the measured fall rate for NIST1C. Curves A–F correspond to nominal measured pressures of 7, 9, 12, 16, 21, and 26 MPa, respectively.

above. A period of about 30 min between two successive pressures was found adequate to allow the system to return to equilibrium, and about 10 min was required to repeat observations at each pressure point.

As it was not possible to bring the two pistons to the same operating reference level during the cross float, a pressure head correction term was applied to compensate for the difference in the operating levels. In the case of the NIST1 and NIST3 gauges, the reference level of the latter was higher by 0.135 m, whereas its reference level was lower by 0.083 m when compared against the NIST2 gauge.

Throughout these studies the piston in the NIST3 test gauge was rotated clockwise with a rotational speed of 35 ± 5 rpm by a pulley system coupled to a dc motor. The NIST1 and NIST2 gauges were manually rotated clockwise so as to maintain the piston rotational speed of 25 ± 10 rpm. A standard pressure transmitting fluid for this pressure range was used.

All piston gauges used were supported by a sturdy wooden base in order to minimize vibration and magnetic effects. All measurements were taken in an environment which provided stable temperature conditions within ± 1 K. The temperature of piston gauges NIST1 and NIST2 were measured with a thermistor, which used a digital display having a resolution of ± 0.01 K, attached to the pressure column containing the piston-cylinder assembly. The temperature of the test gauge was measured with a platinum resistance thermometer attached near the piston, and its output was read with an autoranging digital multimeter having a resolution of ± 0.006 K.

IV. RESULTS AND DISCUSSION

The measured fall rates for NIST1C were taken at 295 K for six discrete measured pressures: 7, 12, 21, and 26 MPa with increasing pressure, and 16 and 9 MPa with decreasing pressure. At least three measurements of the fall rate were made at each jacket pressure for a particular measured pressure, and the jacket pressures are plotted as a function of the cube root of the fall rates in Fig. 2. Extrapolation of each set of data to zero fall rate was done by fitting an equation of the form $[P_j = P_z - B\ (\text{fall rate})^{1/3}]$ to the data. In all cases three standard deviations (3σ) of P_z were within 0.12–0.54 MPa. The stall curve is the plot of P_z vs P_m, and is shown in Fig. 3. This curve allows for choosing an appropriate operating jacket pressure when using the gauge to generate a given nominal measured pressure. Using this value for the jacket pressure along with the pressure-dependent expressions for d and P_z, Eq.

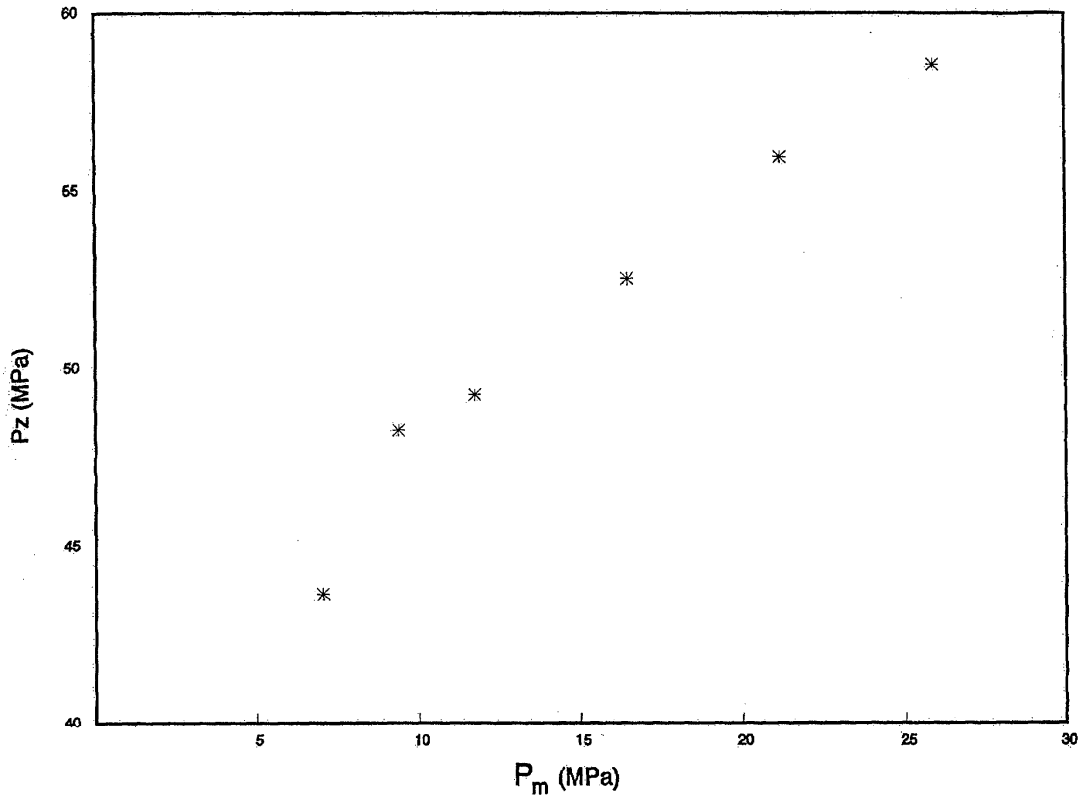

FIG. 3. Graph of zero-clearance jacket pressure (P_z) vs nominal measured pressure (P_m) for NIST1C.

(2) can be used to determine the effective area c the gauge; which can then be used in Eq. (1) to determi the actual generated pressure being measured. During the fall rate measurements, the operating jacket pressures were chosen to obtain fall rates of about 1 mm/h, consistent with a small clearance and reasonably low friction between the piston and the cylinder.

The overall fractional uncertainty in the pressure measured at the reference level of the controlled clearance piston gauge depends on the uncertainty in the individual parameters of Eqs. (1) and (2), and can be expressed as the root-mean square of the total differentials of the individual parameters, x_i (Ref. 2):

$$\frac{dP}{P} = \left[\sum_{i=1}^{n} \left(\frac{1}{P} \frac{\partial P}{\partial x_i} dx_i \right)^2 \right]^{1/2}. \tag{8}$$

The values of the differentials, their uncertainties, and the fractional uncertainties in P_m for NIST1, when used in the controlled clearance mode, are listed in Table I. The overall uncertainty at 296 K and at 26 MPa is 30 ppm (3σ).

The conventional cross float method was used to calibrate the NIST3 test gauge against the NIST1C and NIST2 pressure standards. A computer program developed and used at NIST, which determines the effective area and the pressure coefficients of the test gauge based upon those of the standard, was used to evaluate the data. This program also provides the standard deviation of the residuals of the area, and the standard deviation of the coefficients.

In all the calibrations of the test gauge NIST3 against either the NIST1 or NIST2 pressure standards, three test cycles were carried out. In one cycle the pressure was increased to 7, 11, 16, 21, and 26 MPa, and then decreased from 21 to 7 MPa in similar steps. In the other two cycles, the measurement proceeded from the highest pressure to the lowest, and back to the highest. In one test cycle nine observations were taken, leading to a total of 27 observations per calibration.

The residuals in the effective area of NIST3 as a function of nominal measured pressure, when calibrated against NIST1C, are shown in Fig. 4. This figure gives the deviation of the effective area, in ppm, for the individual measured pressures, from the best low-order fit equation $A_e = A_0(1 + bP)$, where $A_0 = 1.961\,191 \times 10^{-5}$ m^2 and $b = 9.85 \times 10^{-7}$ MPa^{-1}, and P is in MPa. In all subsequent discussion, these values will be considered as the reference values for comparison purposes. Note that while the residuals are not totally random, their magnitude is small enough that their structure is not of immediate concern. Similar scatter in the residuals of the effective area (A_e) of NIST3 is also observed when NIST3 is calibrated against NIST1R and NIST1S$_e$, and so is not represented

TABLE I. Total uncertainty of pressure for NIST1C.

X_i	Value	$\frac{1}{P}\frac{\delta P}{\delta X_i}$	Value	dX_i	$\frac{1}{P}\frac{\delta P}{\delta X_i}dX_i$ (ppm)
M	1.30×10^{2} kg	$1/M$	7.69×10^{-3}/kg	2.8×10^{-4} kg	2.0
g	9.801 018 m/s^2	$1/g$	1.02×10^{-1} s^2/m	5×10^{-6} m/s^2	0.5
ρ_a	1.18 kg/m^3	$1/\rho_m$	1.2×10^{-4} m^3/kg	1×10^{-2} kg/m^3	1.2
ρ_m	8.4×10^{3} kg/m^3	ρ_a/ρ_m^2	1.7×10^{-8} m^2/kg	1×10^{2} kg/m^3	1.7
γ	3.09×10^{-2} N/m	C/gM	1.96×10^{-5} m/N	3×10^{-4} N/m	0
C	2.5×10^{-2} m	γ/gM	2.42×10^{-5}/m	1×10^{-5} m	0
A_0	$4.902\,139\times10^{-5}$ m^2	$1/A_0$	2.04×10^{4}/m^2	3.2×10^{-10} m^2	6.5
α_p	4.5×10^{-6}/°C	$(T-T_r)$	2 °C	3×10^{-7}/°C	0.6
α_c	4.5×10^{-6}/°C	$(T-T_r)$	2 °C	3×10^{-7}/°C	0.6
$(T-T_r)$	$T_r=23$ °C	$\alpha_c+\alpha_p$	9×10^{-6}/°C	2×10^{-2} °C	0.2
b	-5.49×10^{-13}/Pa	P	2.6×10^{7} Pa	1.8×10^{-14}/Pa	0.5
P	2.6×10^{7} Pa	b	5.49×10^{-13}/Pa	1×10^{5} Pa	0
P_z	5.85×10^{7} Pa	d	3.42×10^{-12}/Pa	1.5×10^{6} Pa	5.13
d	3.42×10^{-12}/Pa	(P_z-P_j)	4.64×10^{7} Pa	7.4×10^{-14}/Pa	3.4
P_j	1.21×10^{7} P_z	d	3.42×10^{-12}/Pa	0.7×10^{5} Pa	0.2
A^a	ΔT	α_p	4.5×10^{-6}/°C	2.7×10^{-2} °C	0.1
A^a	α_p	ΔT	3 °C	3×10^{-7}/°C	0.9
	$\frac{\Delta P}{p}=30$ ppm (3σ)				

[a]Uncertainties due to changing the reference temperature from the 20 °C of the dimensional metrology laboratory to the 23 °C of the pressure measurement laboratory.

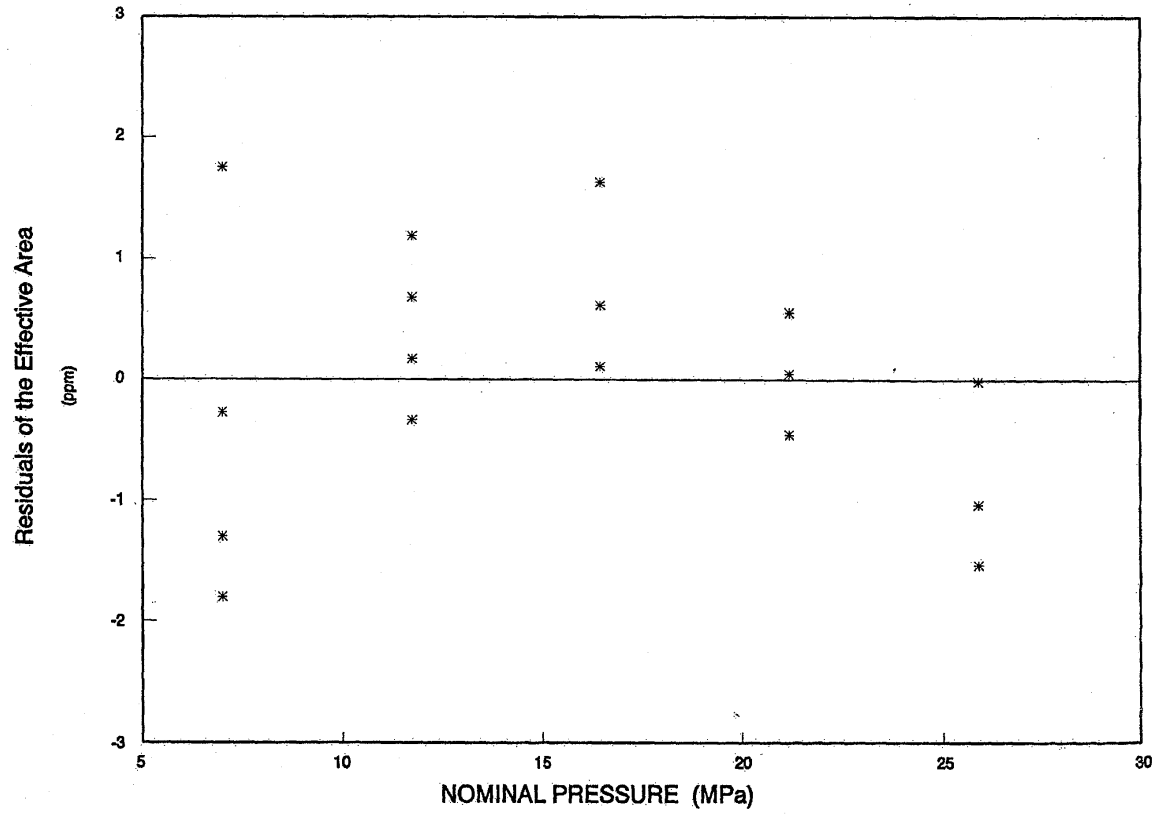

FIG. 4. Deviation of measured values of the effective area (A_e) of NIST3 from the best linear fit, $A_e = 1.961\,191\times10^{-5}(1+9.85\times10^{-7}P)$, when calibrated by NIST1C.

TABLE II. Summary of the calibrations of NIST3 when using NIST1C, NIST1R, NIST1S$_e$, NIST1S$_h$, and NIST2 as the standard gauges.

Operational conditions	A_0 ($\times 10^{-5}$ m^2)	3σ std dev A_0 (ppm)	b (MPa^{-1})	3σ std dev b (MPa^{-1})	3σ std dev A_e (ppm)
1. NIST1C controlled clearance	1.961 191	1.4	9.85×10^{-7}	8.5×10^{-8}	3
2. NIST1R reentrant	1.961 189	2.7	1.54×10^{-6}	1.6×10^{-7}	6
3. NIST1S$_e$ simple	1.961 195	1.6	8.96×10^{-7}	9.2×10^{-8}	4
4. NIST1S$_h$ simple with b value 1.13×10^{-12}/Pa calculated from elastic theory	1.961 189	1.1	1.00×10^{-6}	6.2×10^{-8}	2
5. NIST2	1.961 182	2.5	1.06×10^{-6}	1.2×10^{-7}	4

graphically here. However, the values of the low-pressure effective areas (A_0) and the pressure coefficients (b) of NIST3, along with their 3σ uncertainties, are given in Table II.

The values of A_0 of NIST3 obtained from the calibrations against NIST1R, NIST1S$_h$, and NIST1S$_e$ differ by only 1, 1, and 2 ppm, respectively, from the value obtained from NIST1C. It is clearly evident that all these values agree well among themselves, at a level comparable to the individual 3σ standard deviations in the A_0 coefficients.

The values of b for NIST3 obtained from NIST1S$_e$ and NIST1S$_h$, as given in Table II, differ by -9% and $+1.5\%$ in their absolute magnitude when compared to the absolute value obtained from NIST1C. Considering the 3σ standard deviations of these measured values, these differences are not unreasonable. Additionally, these observed differences cause a relative deviation in the effective area value of only 2 and -0.5 ppm, respectively, at a measured pressure of 7 MPa, which reduces to merely 0.5 ppm at a full-scale pressure of 26 MPa. This rather remarkable agreement supports the model, based on elastic theory, which is used in determining the pressure coefficient of this simple piston-cylinder assembly, and suggests that such calculations should be further investigated in future studies.

Figure 5 shows the effective area of NIST3 when it is measured against NIST1 in its different modes of operation and against NIST2. As the reentrant mode operation of NIST1 leads to a deviant calibration of NIST3, it was decided to investigate the similarity of this calibration to a calibration of NIST3 performed using another NIST pressure standard (NIST2), having a reentrant piston-cylinder assembly. Its metrological parameters are listed in Table III along with the parameters of NIST1 and the derived parameters of NIST3. The NIST2 pressure standard has been calibrated against several other NIST pressure standards, and the closure of the values of the pressure-dependent effective area is well below the systematic uncertainties of the individual standards. The residuals of the effective area of NIST3 as a function of nominal measured pressure, when calibrated against NIST2, are shown in Fig. 6. This gives the deviation of the effective area, in ppm, for the individual measured pressures, from the best-fit equation $A_e = 1.961\,182\times10^{-5}(1 + 1.06\times10^{-6}\,P)$, where A_e is in m^2 and P is in MPa. The value of A_0 agrees within 4.5 ppm, whereas the b value differs by 0.75×10^{-7} MPa^{-1},

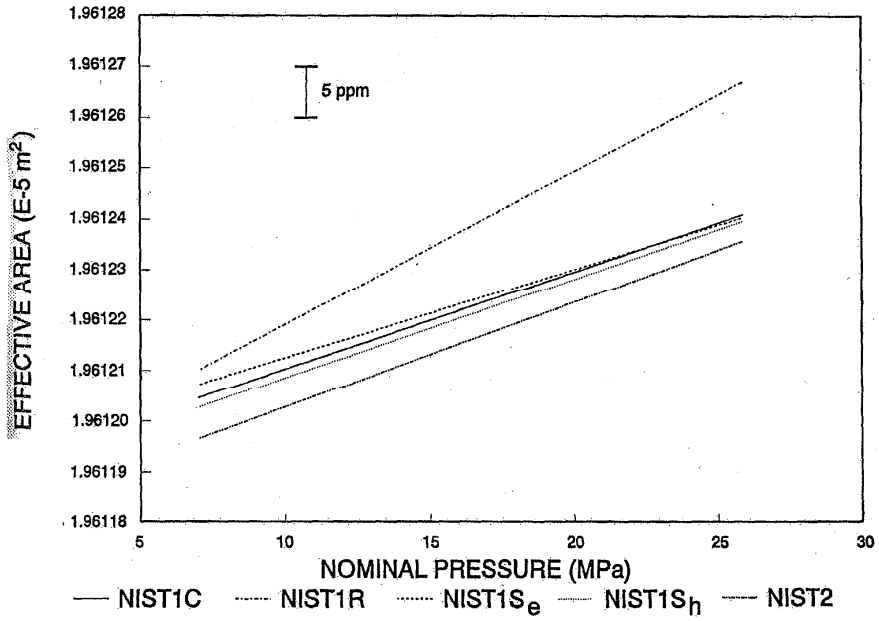

FIG. 5. Effective areas of NIST3 as obtained from the calibrations by NIST2 and NIST1 in its different modes of operation, plotted as a function of pressure. NIST1C: operation of NIST1 in controlled-clearance mode, NIST1R: operation of NIST1 in reentrant mode, NIST1S$_e$: operation of NIST1 in simple mode, NIST1S$_h$: operation of NIST1 in hybrid mode, NIST2: reentrant type pressure standard.

TABLE III. Description of the piston gauges used.

Piston gauge designation	NIST1	NIST2	NIST3
Piston-cylinder type	Controlled, simple, reentrant	Reentrant	Simple deformation
Full-scale pressure (MPa)	28	28	50
Piston material	Tungsten carbide	Tungsten carbide	Tungsten carbide
Cylinder material	Tungsten carbide	Tungsten carbide	Tungsten carbide
Fluid	Standard[b]	Standard[b]	Standard[b]
Coefficient of thermal expansion α_p for piston ($°C^{-1}$)	4.5×10^{-6}	4.11×10^{-6}	4.5×10^{-6}
Coefficient of thermal expansion α_c for cylinder ($°C^{-1}$)	4.5×10^{-6}	4.11×10^{-6}	4.5×10^{-6}
Effective area A_0 at atmosphere pressure at 23 °C (m^2)	$4.902\,813\times10^{-5}$[a]	$8.402\,032\times10^{-5}$	$1.961\,191\times10^{-5}$
Distortion coefficient (Pa^{-1})	1.13×10^{-12}[a]	-2.08×10^{-12}	9.85×10^{-13}
Estimated total uncertainty (3σ) of the effective area $\Delta A_e/A_e$ (ppm)	30[a]	40	35

[a]Simple mode values.
[b]Standard hydraulic pressure transmitting fluid was used.

when compared with the values obtained from NIST1C. Although the value of b differs by 8% in absolute value from the NIST1C value, it is still well within the three-sigma standard deviation of the b coefficient as shown in Table II.

A clearer picture of the intercomparison of the pressure dependent effective area of NIST3, when calibrated against NIST2, and NIST1 in its reentrant mode and simple modes, is presented in Fig. 7, where fractional deviations of the area values from those obtained from NIST1C

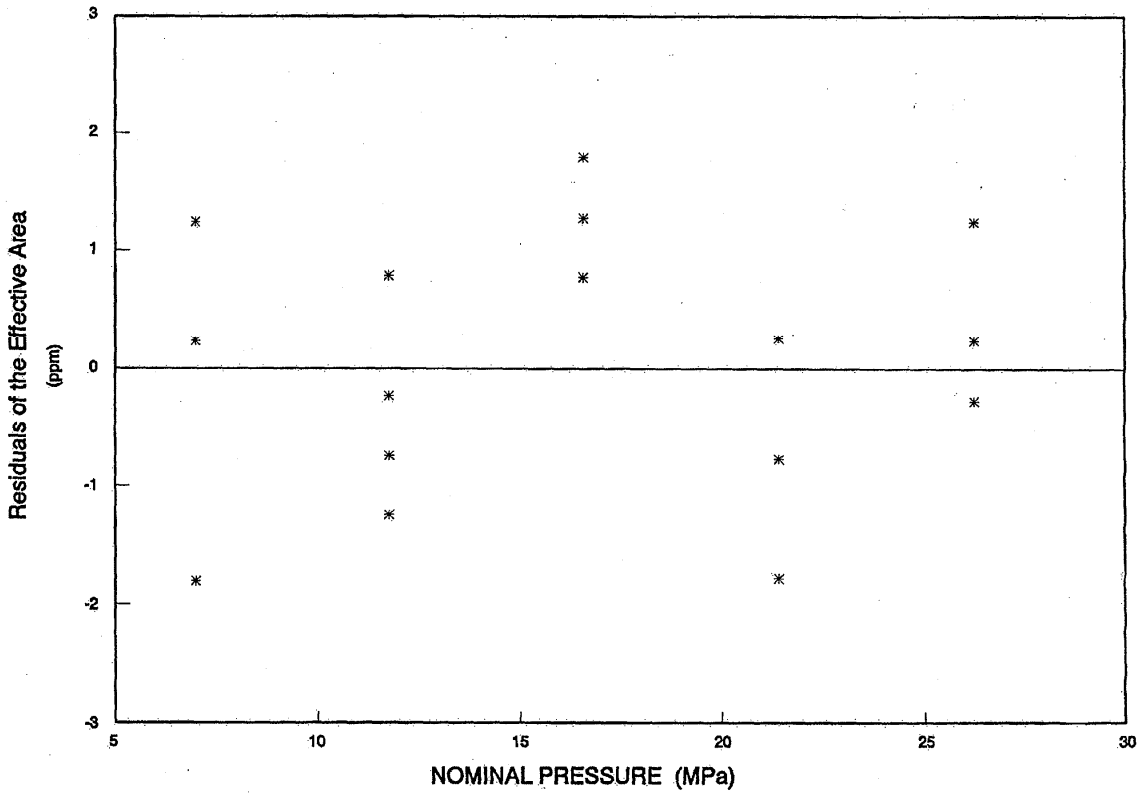

FIG. 6. Deviation of measured values of the effective area (A_e) of NIST3 from the best linear fit, $A_e = 1.961\,182\times10^{-5}(1 + 1.06\times10^{-6}P)$, when calibrated by NIST2.

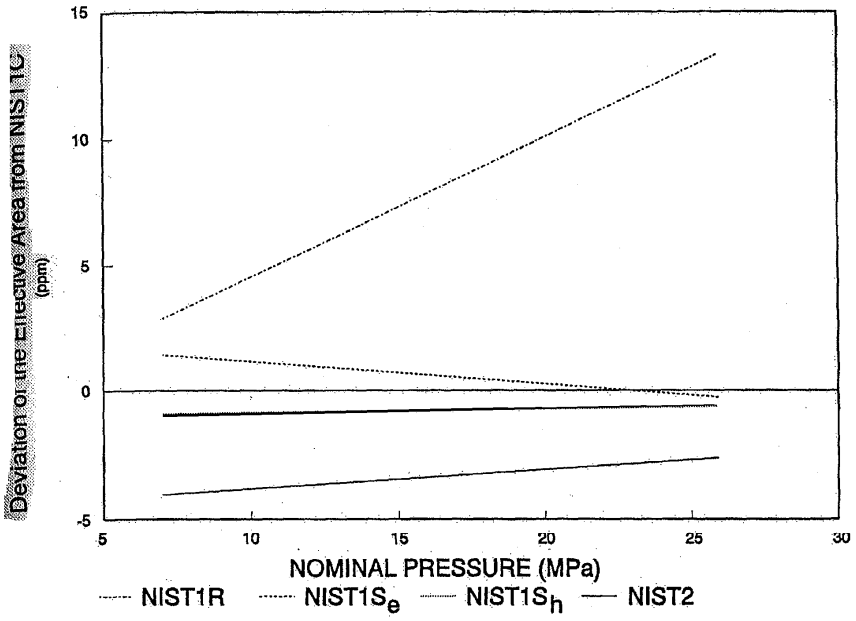

FIG. 7. Deviation of effective areas [Eq. (9)] of NIST3 as a function of nominal measured pressure, obtained from NIST1R: operation of NIST1 in reentrant mode, NIST1S$_e$: operation of NIST1 in simple mode, NIST1S$_h$: operation of NIST1 in hybrid mode, NIST2: reentrant type pressure standard.

are plotted as a function of measured pressure. The fractional change in the effective area is calculated at each measured value according to

$$\frac{\Delta A_e}{A_{e_{\mathrm{NIST1C}}}} = \frac{(A_e)_x - (A_e)_{\mathrm{NIST1C}}}{(A_e)_{\mathrm{NIST1C}}}, \tag{9}$$

where $(A_e)_x$ is the effective area of NIST3 from the calibration of NIST1 or NIST2. Note that the majority of the observed difference between the NIST2 and NIST1C values comes from the difference between their A_0's, and not from the relatively small difference between their b values. It can be seen from a comparison of the data in Fig. 7 with the estimated total uncertainties of the individual gauges given in Table III that the maximum variation in the effective area of NIST3 is smaller than any of the individual total uncertainties.

From Fig. 7 it is seen that the pressure-dependent effective areas of NIST3 obtained from the calibration of NIST2, NIST1S$_e$, or NIST1S$_h$ agree among themselves within 5 ppm, which is well within their 3σ standard deviations. For NIST1R, the value of A_e differs by 14 ppm at 26 MPa. The observed difference in the latter case may be due to NIST1 being operated with values of jacket pressure, which is the same as the measured pressure in this case, which are too high and lie off the linear portion of the fall rate curves that were presented in Fig. 2. Operating at jacket pressures P_j that are off the linear portion of the fall rate curve implies operating conditions that are not consistent with current controlled-clearance piston gauge theory, on which Eq. (2) is based. Thus the use of Eq. (3), which is derived from Eq. (2), is suspect under these conditions. However, the maximum deviation in the effective areas of NIST3, including the calibration against NIST1R, is still less than the individual total uncertainties of the standards used. This study then indicates that controlled-clearance piston gauges, once characterized, may perhaps be used in the simple mode using the controlled-clearance coefficients without significant loss of measurement uncertainty if similar operating conditions are used.

ACKNOWLEDGMENTS

The authors would like to acknowledge the assistance of Mr. Donald Ward for his extensive data reduction and graphics preparation, Dr. Vern Bean for his useful suggestions in the early stage of this investigation, and Dr. J. K. N. Sharma for his support. One of the authors (K. J.) is grateful to the director of the National Physical Laboratory for allowing him to work at NIST.

[1] R. S. Dadson, S. L. Lewis, and G. N. Peggs, *The Pressure Balance: Theory and Practice* (National Physical Laboratory, Teddington, England, HMSO, 1982).
[2] P. L. M. Heydemann and B. E. Welch, in *Experimental Thermodynamics*, edited by B. Le Neindre and B. Vodar (Butterworths, London, 1975), Vol. II, pp. 147–202.
[3] J. C. Legras, G. F. Molinar, K. Schmalhofer, J. K. N. Sharma, M. Thrane, and D. B. Walker, BIPM Internal Report-90/10, 1990.
[4] R. Maghenzani, G. F. Molinar, L. Marzola, and R. K. Kulshreshta, Phys. E 20, 1173 (1987).
[5] J. K. N. Sharma and Kamlesh K. Jain, Pramna 27, 417 (1987).